Model predictive control of interleaved dc-dc stage for photovoltaic microconverters

Jaime Zapata, Samir Kouro, Matias Aguirre, Thierry Meynard

Model predictive control of interleaved dc-dc stage for photovoltaic microconverters

Jaime W. Zapata, Samir Kouro, Matias Aguirre
Electronics Engineering Department
Universidad Tecnica Federico Santa Maria
Valparaiso, Chile
Email: jaime.zapataa.13@sansano.usm.cl, samir.kouro@ieee.org

Thierry Meynard
Institut National Polytechnique de Toulouse
University of Toulouse
Toulouse, France
Email: thierry.meynard@laplace.univ-tlse.fr

***Abstract*—The development of different configurations and topologies implemented in photovoltaic (PV) plants have made possible the increase of efficiency of the system. The traditional configurations of grid-connected PV systems, centralized, string, multi-string and ac-module, have been analyzed and actually most of them are controlled using classic PI control. Furthermore, each of them has different efficiency values due to the inherent associated problems. The large-scale PV plants do not work properly when the modules do not work at the same conditions, for example when some atmospheric and environmental problems are involved, it reduces the reliability of the system. The traditional small-scale PV configurations have a low efficiency due to the dc-boosting stage in order to reach the grid levels. This work presents a grid-connected PV configuration, focused in the improve of the efficiency of the traditional ac-module configuration, a flyback topology for the dc-side and a H-bridge topology for the grid connection will be implemented. Moreover, the proposed control scheme is based on FCS-MPC algorithm.**

I. Introduction

Photovoltaic (PV) technology is well established as a reliable and economical source of electricity, which is gaining more importance due to the increasing power demand in the world, and it has experienced the fastest growth over the last years due to the cost reduction of PV modules.

Depending on the PV applications and power levels, it is possible to group the grid-connected PV systems in different configurations, from a concentrated structure, with a single inverter stage implemented in large-scale PV plants, to a completely distributed structure, which increase the control flexibility. The distributed structures have reached an increasing interest oriented to small-scale PV systems [1].

PV systems without transformers would be the most suitable option in order to minimize the cost of the total system, on the other hand, the cost of the grid-connected inverter is becoming more visible in the total system price. Therefore, the centralized converters are a good option for large-scale PV systems. However, when isolated converters are required, the whole converter size increases, and it leads to a reduction of efficiency with traditional configurations.

Actually, the linear control techniques are implemented in power converters for PV applications. However, in high power converters, some techniques based on predictions of the variable behavior have been proved. Therefore, this work presents two different configurations for small scale PV systems. Furthermore, model predictive control (MPC) technique is developed.

This paper is organized as follows: The alternatives of grid-connected PV system configurations are presented in section II. The traditional ac-module and the proposed configuration

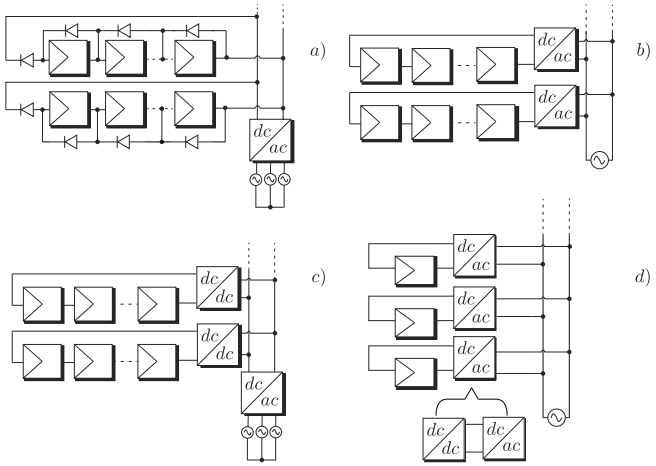

Fig. 1. Traditional grid-connected PV system configurations. a) Centralized. b) String. c) Multi-string. d) Ac-module.

are presented in section III. The control schemes are presented in section IV. The simulation results are shown in section V, and finally in section VI some conclusions are given.

II. Grid-Connected PV System Configurations

Either in standalone configurations or grid-connected systems, PV systems are implemented [2]. The first one is focused on the self consumption of the produced energy depending on the load specifications. The second aims to supply energy to the grid.

Depending on the size of the PV plants, the traditional grid-connected PV systems are grouped in four configurations. Centralized configuration for large-scale PV systems, multi-string configuration for large and medium-scale, string configuration for medium and small-scale systems, and ac-module configuration for small-scale systems.

Large scale PV systems are commonly grid-connected using a central three phase voltage source inverter, this is the main feature of the centralized configuration. The topology is shown in Fig. 1 a). The whole PV system is connected to the inverter. Using a string configuration, which is the series connection of single PV modules, in order to achieve the desired dc-link voltage. Parallel connection of some strings are made, in order to reach the power rating. It presents some drawbacks due to the central inverter topology; there are a single MPPT, therefore in partial shading scenarios there are significantly reduction of produced power. Blocking and bypass diodes are required [3].

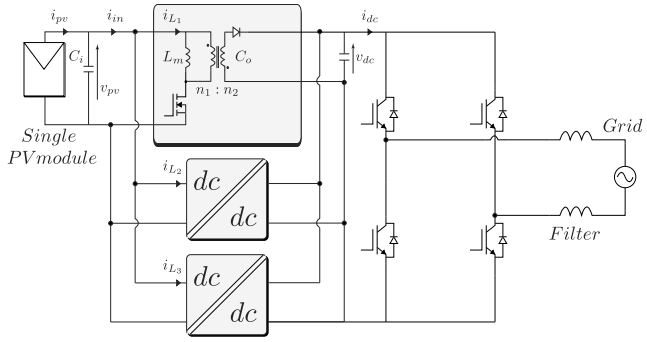

Fig. 2. Ac-module PV system based on interleaved flyback converters and H-bridge inverter [5].

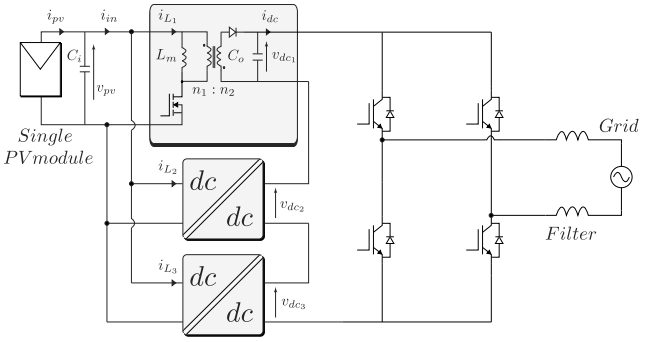

Fig. 3. Proposed parallel to series interleaved ac-module converter.

String configuration is a reduced version of the centralized topology so that, it uses one inverter per PV string as shown in Fig. 1 b), therefore the series blocking diode is not needed. The input voltage is high enough to avoid an elevation stage and a separate MPPT can be applied to each string. The main drawbacks of this topology are the higher component count, this means several individual control systems, and more magnetic components if galvanic isolation is required.

Multi-string configuration is shown in Fig. 1 c). This topology combines the advantage of higher energy yield of a string inverter with the lower costs of a central inverter [3]. The multi-string configuration allows an individual MPPT in the dc-dc stage, a voltage elevation and isolation if is required, therefore it is possible to implement it in medium and small-scale PV plants keeping a high efficiency.

Finally, the small-scale PV plants use the ac-module topology for the single-phase grid connection as shown in Fig. 1 d). It has one converter connected to each PV module in order to do the MPPT. The losses produced by the partial shading are reduced, however the efficiency of the whole system is the lowest. This problem is the required voltage elevation stage for the grid-connection, therefore, this topology is only implemented in small-scale PV plants.

III. Module integrated converters

The small-scale PV systems, like rooftops applications, had increased considerably in the last years. Therefore, the module integrated converters (MIC) configuration is one of the most recent approach to grid connection. This configuration has two steps. The dc-stage is formed by micro-dc converters that are made in order to do the maximum power point tracking (MPPT), boost the dc voltage, and provide galvanic isolation if is required. In order to connect to the grid a dc-ac inverter is required, it eliminates all dc high voltage wiring. The MIC configuration are generally at cost disadvantage compared to other approaches [4], but actually the semiconductors and power converters development has made this configuration increasingly competitive.

A. Interleaved input & Interleaved output connection

The commercial ac-module configuration was developed by Enphase Energy [5], currently commercialized by Siemens. The most common configuration is shown in Fig. 2. It works with the flyback micro-dc converter and H-bridge micro-inverter topology. The main feature of this configuration is the interleaved flyback converters. With these connection the power is divided by the number of converters, enabling higher switching frequencies, and it allows a reduction in the size of the HF-transformer. This configuration works using phase shifted carriers for reference modulation stage. It allows a reduction in the current ripple, extending the lifespan of the capacitors [6].

Because of the dc-boost stage, it configuration has the lowest efficiency compared with the other grid-connected configurations, since the voltage ratio conversion is higher between the output PV module and the grid.

B. Interleaved input & Series output connection

The proposed configuration is shown in Fig. 3. It works with the flyback micro-dc converter and H-bridge micro-inverter topology. It has the same advantages that were mentioned before due to the interleaved concept. Moreover, the series output connection reaches the required voltage level to the dc-ac inverter, with a lower voltage distribution at output of the flyback converters, for that reason, the conduction and commutation losses are lower compared with the interleaved output configuration, leading an efficiency increase. Furthermore, the reduction of capacitors size is considerably due to the reduced voltage levels, hence the reduction of the converter design.

IV. Control algorithms

The flyback converter is used in low-power applications, therefore it is suitable for the studied case. The main feature of this topology is shown in the following equation. It is possible to notice the buck and boost feature.

$$n_t = \frac{n_1}{n_2}$$

$$\frac{V_o}{V_i} = \frac{D}{n_t(1-D)} \tag{1}$$

where,
n_1 : number of turns of primary winding.
n_2 : number of turns of secondary winding.
V_o : output voltage.
V_i : input voltage.
D : duty cycle.

As shown in (1), it is possible to notice that depending on the duty cycle, either the input voltage or the output voltage, can be controlled.

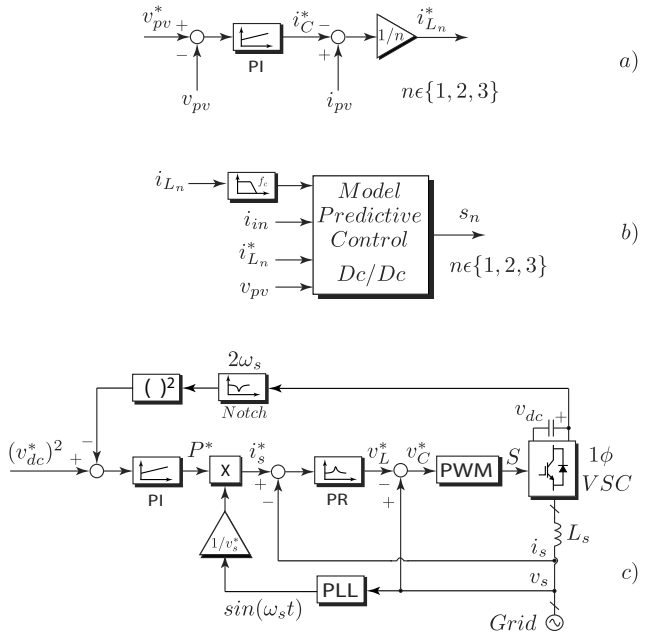

Fig. 4. Control scheme. a) Voltage control scheme. b) Current control scheme. c) Single-phase voltage oriented control.

A. Classic PI for voltage control at MPP

In literature is easily to find many dc-dc converter controllers depending of the topology and the power converter model. One of traditional control scheme to develop the voltage control at mpp is shown in 4 a).

The outer control loop receive the voltage reference v^*_{pv} obtained from the MPPT algorithm, in this case, perturb and observe ($P\&O$) is implemented due to the simple design. It is compared with the measured voltage in the input capacitor and the error is controlled using a linear proportional-integral (PI) controller. The output signal is the current through the input capacitor i^*_C, but the aim is to control the current through the inductor in order to remain a continuous conduction mode, therefor a feed-forward compensation loop is included, the reference given is the inductor current per each cell $i^*_{L_n}$. It is divided by the number of dc converters n, and compared with measured current of each cell. The feedback current is filtered at the switching frequency, so that it generates an imbalance in the capacitors when the filter is not included.

B. FCS-MPC for current control

When PI controllers are used to operate dc-dc converters a linear cascaded control loop is required. Moreover, to reduce the current ripple at input on interleaved connections, the carriers for each converter are shifted in phase by $2\pi/n$ [rad], where n is the number of interleaved converters.

Finite control set model predictive control (FCS-MPC) is a simple method, which allows the control of different converters and variables without the need to implement cascaded control loops or modulation techniques [7]. The last one is the main advantage at the proposed converter compared with traditional linear control methods with modulator, because if increases the number of converters, the carrier signals required for the modulation techniques also increase.

In order to model the flyback converter, the equations for each commutation states of the switching device are obtained.

when, $s = 1$:

$$v_{pv} = L_m \frac{di_L}{dt} \tag{2}$$

when, $s = 0$:

$$L_m \frac{di_L}{dt} = -n_t v_{dc} \tag{3}$$

In order to implement the control algorithm, the behavior of control variable is predicted at next sampling time k by deriving the equations in discrete time. However, it is possible to extend to n-step p in prediction horizon. Further, both equations are expressed as one equation which depends on the switching state s.

$$i^{\rightarrow}_L(k+p+1) = i^{\rightarrow}_L(k+p) + s\frac{T_s}{L_m}v_{pv}(k) - (1-s)\frac{T_s}{L_m}n_t v_{dc} \tag{4}$$

where,

$i^{\rightarrow}_L \epsilon \{i_{L1}, i_{L2}, i_{L3}\}$. They are the input currents for each dc-converter.

However, using the sampling instant $k+2$ the calculation delay is compensated [8].

With the calculated predictions it is possible to define a cost function, it will be minimized in order to achieve the smaller error. The chosen cost function structure is the quadratic function of the error as shown,

$$g1 = (i^*_L(k) - i^{\rightarrow}_L(k+2))^2 \tag{5}$$

C. Frequency fixing & Ripple control

In order to achieve the control objective with classic predictive algorithms, a high switching frequency is required. It means that the switching losses also increase. There are methods to improve the efficiency without affecting the performance of the system. These are implemented in order to reduce the switching frequency and improve the converter design, either in matrix converters [9], or when interleaved boost converters are used [10].

The fixed frequency algorithm is based on the counting samples that have passed since the last commutation $M(k)$ and the predicted samples depending of the different switching states $M(k+1)$. Considering this term, the cost function is the following.

$$g2 = (M^*(k) - M(k+1))^2 \tag{6}$$

The given reference is based on the desired switching frequency

$$M^*(k) = \frac{f_c}{2f_r} \tag{7}$$

where, f_c is given by the sample frequency, and f_r by the reference frequency.

One advantage of the interleaved connections is the reduction of the current ripple. When PI controllers with modulation techniques are implemented, it is possible to minimize the ripple using phase shifted carriers. But the associated problem is that increasing interleaving converters, also increase the required carriers.

It is possible to aim a similar effect with FCS-MPC. Despite of modulation techniques are not implemented, the switching pulses are chosen in order to minimize the total input current ripple. The cost function has the following structure.

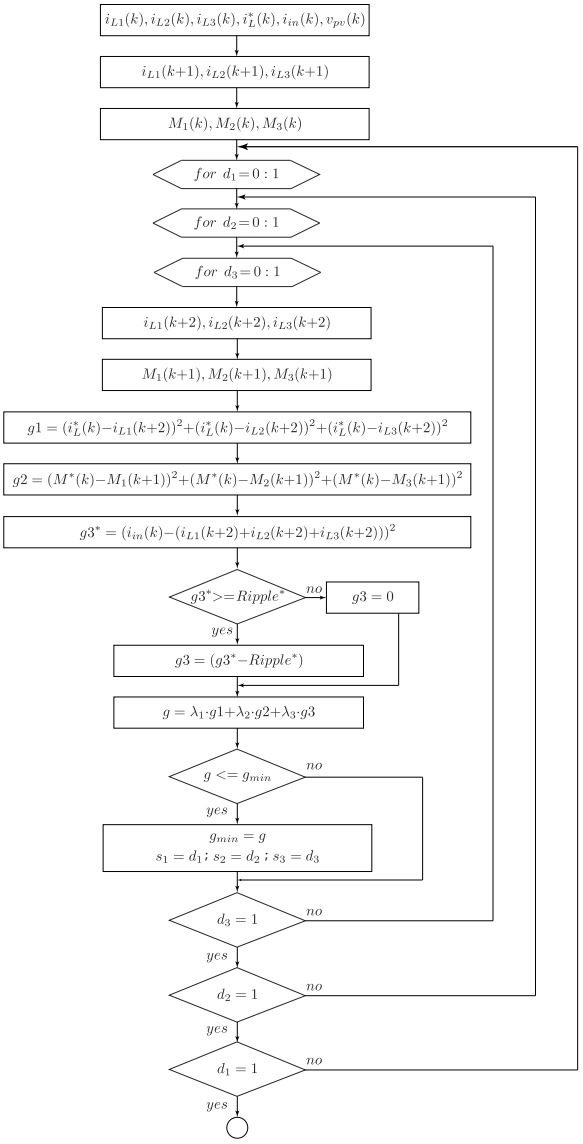

Fig. 5. Flow diagram for current and ripple control with fixed frequency using FCS-MPC.

$$g3 = max[0, (i_{in}(k) - \sum_{j=1}^{n} i_{Lj}(k+2))^2 - Ripple^*] \quad (8)$$

The global cost function is represented as the following equation.

$$g = \lambda_1 \cdot g1 + \lambda_2 \cdot g2 + \lambda_3 \cdot g3 \quad (9)$$

The weight factors are chosen in order to escalate the errors between the different variables and make them comparable.

The flow diagram of the proposed FCS-MPC is shown in Fig. 5.

In Fig. 6 a) the current spectrum is shown. It is possible to see the current harmonics around the fixed switched frequency, and around the multiples of this frequency.

In Fig. 6 b) the input current in each converter is shown. The shifted is made in order to obtain the minimum total input current ripple.

D. Single-phase voltage oriented control

While the flyback converter is implemented in order to achieve the desired dc-link voltage, H-bridge inverter topology

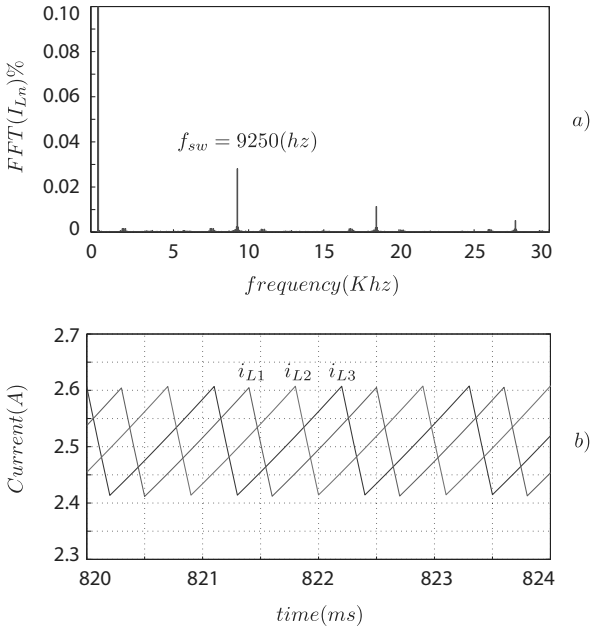

Fig. 6. Input current results. a) Current spectrum under fixed frequency. b) Input current in each converter.

is used in order to control the dc-link voltage, grid synchronization and active/reactive power control. When the control is focused in a three-phase grid connection, the dq reference frame transformation is implemented, enabling the use of PI controllers. Nevertheless, this transformation is not possible to implement when the goal is the single-phase grid connection, but the VOC is adapted by synchronizing the grid current reference directly with the single-phase grid voltage [11].

The single-phase VOC scheme is shown in Fig. 4 c). The voltage outer loop is controlled using a PI which compares the error between the reference and the measured dc-link voltage. Notice that the implemented notch filter is important in the loop so that there is a strong second harmonic due to the rectification. The output signal of the controller is the active power reference P^* and it is divided by the grid voltage amplitude to obtain the grid current reference i_s^*. The phase is obtained with a PLL structure and, the advantage of this, is to avoid the introduction of grid harmonics. The current reference has a sinusoidal waveform, therefore a proportional resonant (PR) controller is implemented. The output signal of the controller is the grid filter inductor voltage reference v_L^*. The converter voltage reference V_C^* is obtained implementing a feedforward compensation, and this signal is modulated using a PWM strategy to obtain the gate drive signal for the semiconductors.

V. Simulation Results

In order to validate the configuration, a comparison was made between the interleaved flyback converters connected in parallel at the input and output and the proposed one. The simulation parameters are shown in the Table I.

A. Interleaved input & Interleaved output ac-module configuration

The results are shown in Fig. 7. A solar irradiance change is made at $t = 1.0[s]$ in order to evaluate the dynamic behavior. In Fig. 7 a) the input voltage v_{pv} is shown. $P\&O$ is the selected algorithm to do the MPPT, due to the ease

TABLE I
SIMULATION PARAMETERS

Variable	Parameter	Value
P_{pv}	PV module peak power	240 [W]
V_{mpp}	PV voltage at maximum power point	29.5 [V]
G_{stc}	Solar irradiance at STC	1000 [W/m^2]
T_{stc}	Temperature at STC	25 [^{o}C]
V_s	Grid voltage	220 [V_{rms}]
L_s	Grid filter	10 [mH]
C_i	Input capacitor	220 [μF]
C_o	Dc-link capacitor	2200 [μF]
f_{1sw}	Dc-Ac switching frequency	3 [KHz]

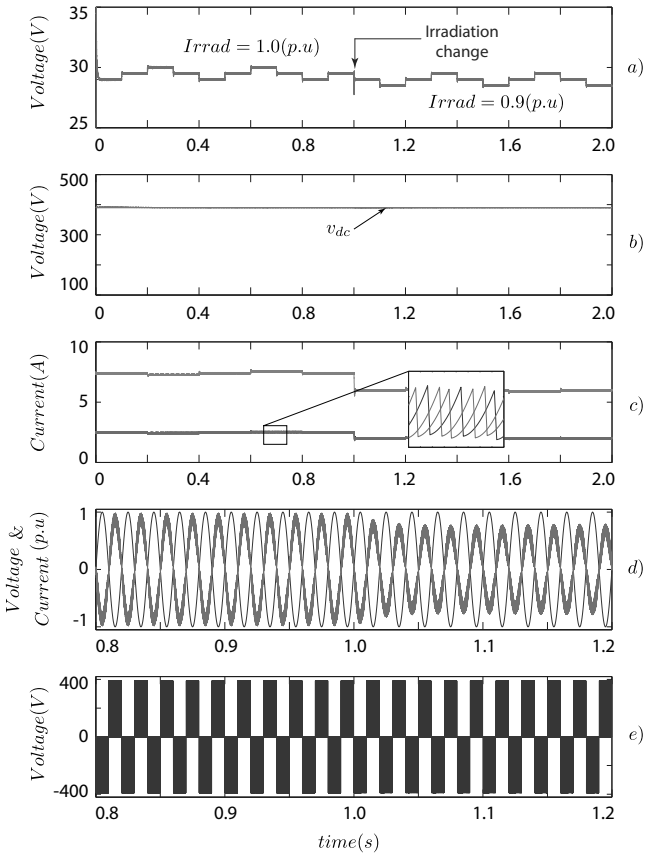

Fig. 7. Interleaved input & Interleaved output connection. a) PV voltage. b) Dc-side output voltage. c) Input current. d) Grid voltage and current. e) Converter voltage.

implementation and good behavior when there are not rapidly changes in solar irradiance variations.

Fig. 7 b) shows the dc-link voltage, due to the inverter dc-ac stage, the required dc voltage is at least 20% more than the grid voltage. Therefore, each one of the dc-dc converters needs to elevate a high voltage ratio, it is directly associated with losses. Moreover, the output capacitor must to be sized for the whole voltage, increasing the converter size.

Fig. 7 c) shows the input current in each converter and the total input current. The shifted between the currents are highlighted.

Fig. 7 d) shows the voltage and grid current, the waveform shows a sinusoidal feature with unity power factor, the inner loop of the single-phase VOC is the responsible to achieve this aim while the outer loop keeps the dc-link in the desired level.

Fig. 7 e) shows the three levels in the voltage generated by the converter.

B. Interleaved input & Series output ac-module configuration

The results are shown in Fig. 8. A solar irradiance change is made at $t = 1.0[s]$, as the same way that the evaluation mentioned before, in order to evaluate the dynamic behavior. In Fig. 8 a) the input voltage v_{pv} is shown. Perturb and observe ($P\&O$) is the selected algorithm for performing the MPPT.

Fig. 8 b) shows the dc-link voltage and the dc-voltage generated per each cell. Due to the inverter dc-ac stage, the required dc voltage is at least 20% more than the grid voltage as mentioned before. The main difference with the traditional ac-module configuration is that the output voltage is divided by the number of cells. Therefore, the voltage ratio elevation is lower, and depending of the cells number in series connection, is possible to reduce it more. The advantage of this configuration is that the output capacitors reduce their size due to the low voltage, and the switching frequency in the dc-dc converter could be controlled with the implemented control strategy, in order to increase the frequency whereas the size of the magnetic components is reduced.

Fig. 8 c) shows the input current in each converter and the total input current. The shifted between the currents are highlighted.

Fig. 8 d) shows the voltage and grid current, this waveform is not different to the configuration shown before because of the single-phase VOC works with the full power, which is independent of the number of cells, and the control schemes are isolated between them.

Fig. 8 e) shows the three levels in the voltage generated by the converter.

C. Analysis of efficiency

In simulation process, generally the analysis is made using ideal power electronic components, however, in order to evaluate the efficiency between both connections, the model of thermal losses is implemented in each semiconductor in order to get the conduction and commutation losses.

To analyze the diode losses, the conduction and switching losses are modeled using the following equations [12], and it is implemented in the simulation.

$$P_{cond} = v_d \cdot i_F \tag{10}$$

$$P_{sw\_off} = E_{rr} \cdot f \tag{11}$$

where,
v_d : diode voltage drop.
i_F : diode forward current.
E_{rr} : reverse recovery energy losses.
f : switching frequency.

The losses are modeled depending on the specifications for each component, therefore, it is possible to find other models based on other devices information. To analyze the mosfet and igbt's losses, the model is made with the following equations.

$$P_{cond} = v_{ce,ds} \cdot i_{c,d} \tag{12}$$

$$P_{sw_{on}} = E_{on} \cdot f \tag{13}$$

$$P_{sw_{off}} = E_{off} \cdot f \tag{14}$$

where,
$v_{ce,ds}$: collector-emitter/drain-source voltage.

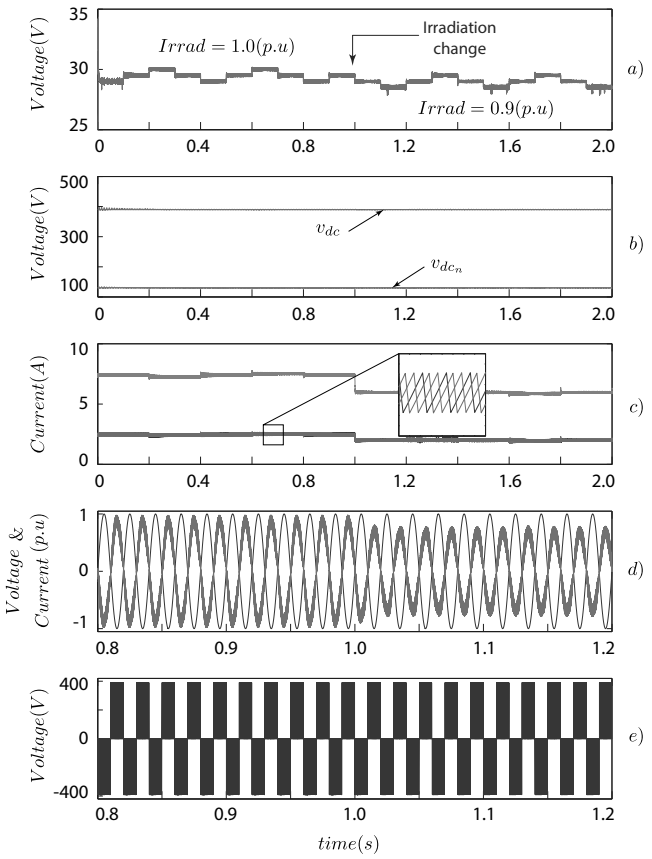

Fig. 8. Interleaved input & Series output connection. a) PV voltage. b) Dc-side output voltage. c) Input current. d) Grid voltage and current. e) Converter voltage.

$i_{c,d}$: collector/drain current.
E_{on} : turn-on energy losses.
E_{off} : turn-off energy losses.

The energy models depend on the required accuracy. The implemented model is based on the turn-on and turn-off times obtained from the component specifications, and a simple model is presented in the following equations.

$$E_{on} = v_{ce,ds} \cdot i_{c,d} \cdot t_{on} \tag{15}$$

$$E_{off} = v_{ce,ds} \cdot i_{c,d} \cdot t_{off} \tag{16}$$

The proposed models work with a specific temperature, usually the standard test conditions are $25^o[C]$, it depends on the manufacturer information.

Fig. 9 shows the results at different irradiance level. The losses are directly related with the voltage ratio elevation in the dc-dc conversion stage, therefore, the interleaved input and series output connection, of micro-dc converters for ac-module configuration, shows a higher efficiency.

VI. Conclusions

Two different output connections of micro-dc converters were evaluated in this work, and it was controlled using a model predictive control algorithm. The traditional interleaved connection presents a lower efficiency than the proposed connection, which has a lower elevation ratio in the dc side. However, the output series connection allows a higher dc output voltage with a greater efficiency. Moreover, since the predictive algorithm performs the current control, modulation techniques are not required. In order to minimize the input current ripple, a fixed frequency technique and a ripple control are developed, which is necessary to improve the design of the converter and reduce the magnetic components sizing.

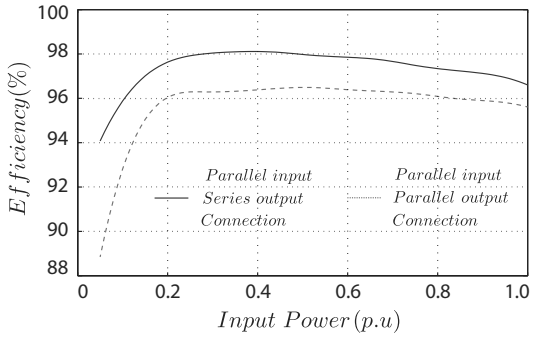

Fig. 9. Converter efficiency at different irradiance level.

VII. Acknowledgment

The authors acknowledge the support provided by FONDECYT Project 1151426, CONICYT/MEC Project 80130057, by SERC Chile (CONICYT/FONDAP/15110019) and by AC3E (CONICYT/FB0008) of Universidad Tecnica Federico Santa Maria.

References

[1] S. Kouro, J. Leon, D. Vinnikov, and L. Franquelo, "Grid-connected photovoltaic systems: An overview of recent research and emerging pv converter technology," *Industrial Electronics Magazine, IEEE*, vol. 9, no. 1, pp. 47–61, March 2015.

[2] G. Walker and J. Pierce, "Photovoltaic dc-dc module integrated converter for novel cascaded and bypass grid connection topologies - design and optimisation," in *Power Electronics Specialists Conference, 2006. PESC '06. 37th IEEE*, June 2006, pp. 1–7.

[3] M. Calais, J. Myrzik, T. Spooner, and V. Agelidis, "Inverters for single-phase grid connected photovoltaic systems-an overview," in *Power Electronics Specialists Conference, 2002. pesc 02. 2002 IEEE 33rd Annual*, vol. 4, 2002, pp. 1995–2000.

[4] J. Myrzik and M. Calais, "String and module integrated inverters for single-phase grid connected photovoltaic systems - a review," in *Power Tech Conference Proceedings, 2003 IEEE Bologna*, vol. 2, June 2003, pp. 8 pp. Vol.2–.

[5] M. Fornage, "Method and Apparatus for Converting Direct Current To Alternating Current," US patent 2007/0221267A1, 2007.

[6] S. Kouro, B. Wu, H. Abu-rub, and F. Blaabjerg, "Photovoltaic Energy Conversion systems," in *Power Electronics for Renewable Energy Systems, Transportation, and Industrial Applications*, 1st ed. IEEE/Wiley, 2014, ch. 7.

[7] S. Kouro, P. Cortes, R. Vargas, U. Ammann, and J. Rodriguez, "Model predictive control a simple and powerful method to control power converters," *Industrial Electronics, IEEE Transactions on*, vol. 56, no. 6, pp. 1826–1838, June 2009.

[8] P. Cortes, J. Rodriguez, C. Silva, and A. Flores, "Delay compensation in model predictive current control of a three-phase inverter," *Industrial Electronics, IEEE Transactions on*, vol. 59, no. 2, pp. 1323–1325, Feb 2012.

[9] R. Vargas, U. Ammann, and J. Rodriguez, "Predictive approach to increase efficiency and reduce switching losses on matrix converters," *Power Electronics, IEEE Transactions on*, vol. 24, no. 4, pp. 894–902, April 2009.

[10] M. Aguirre, S. Kouro, J. Rodriguez, and H. Abu-Rub, "Model predictive control of interleaved boost converters for synchronous generator wind energy conversion systems," in *Industrial Technology (ICIT), 2015 IEEE International Conference on*, Mar 2015.

[11] R. Teodorescu, M. Liserre, and P. Rodriguez, *Grid Converters for Photovoltaic and Wind Power Systems*. IEEE/Wiley, 2011.

[12] G. Vazquez, T. Kerekes, A. Rolan, D. Aguilar, A. Luna, and G. Azevedo, "Losses and cmv evaluation in transformerless grid-connected pv topologies," in *Industrial Electronics, 2009. ISIE 2009. IEEE International Symposium on*, July 2009, pp. 544–548.